

Excitonic effects in energy loss spectra of freestanding graphene

Alberto Guandalini,^{*,†,‡} Ryosuke Senga,[¶] Yung-Chang Lin,[¶] Kazu Suenaga,^{¶,§}
 Andrea Ferretti,[†] Daniele Varsano,[†] Andrea Recchia,^{||,‡} Paolo Barone,^{⊥,‡}
 Francesco Mauri,[‡] Thomas Pichler,[#] and Christian Kramberger[#]

[†]*S3 Centre, Istituto Nanoscienze, CNR, Via Campi 213/a, Modena (Italy)*

[‡]*Dipartimento di Fisica, Università di Roma La Sapienza, Piazzale Aldo Moro 5, I-00185
 Roma, Italy*

[¶]*Nanomaterials Research Institute, National Institute of Advanced Industrial Science and
 Technology (AIST), Tsukuba 305-8565, Japan*

[§]*The Institute of Scientific and Industrial Research (SANKEN), Osaka University
 Mihogaoka 8-1, Ibaraki, Osaka 567-0047, Japan*

^{||}*Center for Life NanoScience, Istituto Italiano di Tecnologia, viale Regina Elena 291,
 00161 Rome, Italy*

[⊥]*CNR-SPIN, Area della Ricerca di Tor Vergata, Via del Fosso del Cavaliere 100, I-00133
 Rome, Italy*

[#]*University of Vienna, Faculty of Physics, Strudlhofgasse 4, A1090, Austria*

E-mail: alberto.guandalini@uniroma1.com

Abstract

In this work we perform electron energy-loss spectroscopy (EELS) of freestanding graphene with high energy and momentum resolution to disentangle the quasielastic

scattering from the excitation gap of Dirac electrons close to the optical limit. We show the importance of many-body effects on electronic excitations at finite transferred momentum by comparing measured EELS with ab initio calculations at increasing levels of theory. Quasi-particle corrections and excitonic effects are addressed within the GW approximation and Bethe-Salpeter equation, respectively. Both effects are essential in the description of the EEL spectra to obtain a quantitative agreement with experiments, with the position, dispersion, and shape of both the excitation gap and the π plasmon being significantly affected by excitonic effects.

Introduction

Since its discovery^{1,2}, the electronic excitations in graphene have been extensively studied because of their relevance for plasmonics and optoelectronics³⁻⁶. Electron energy loss (EEL) spectroscopy (EELS) resolved both in energy and momentum is a powerful tool to investigate dispersion relations of electronic excitations, as it directly probes the dynamical inverse dielectric function (i.e. the energy-loss function) which provides information on both collective longitudinal excitations (plasmons) and electron-hole pair excitations. The energy loss function of undoped graphene and of related sp^2 carbon materials, graphite and nanotubes, always display π and $\pi + \sigma$ plasmons, arising from interband transitions occurring below 10 eV and above 15 eV, respectively⁷⁻¹². Dimensionality affects their dispersion relations via interlayer Coulomb interaction, resulting in a parabolic dependence on the momentum of the π plasmon in graphite⁸, as opposed to its linear dispersion measured in single-wall nanotubes¹² and freestanding single-layer graphene^{9,10}.

Besides plasmons, undoped graphene displays electron-hole pair excitations due to interband transitions between lower and upper Dirac cones³, resulting in a momentum-dependent onset of the EEL spectra. Its direct measurement has been so far elusive due to the background of non-scattered electrons, concealing low-energy features within the zero-loss peak in experiments. On the other hand, interband transitions have been experimentally inferred

from the linewidth of graphite surface plasmons, decreasing with increasing in-plane momentum transfer as the electron-hole continuum is more and more gapped, thus reducing the number of possible plasmon decay-channels into electron-hole excitations¹³.

Inelastic X-ray scattering measurements of graphite have also been used to extract longitudinal excitations in graphite by removing the Coulomb interaction between the layers from the graphite response^{14,15}. However, low-energy excitonic effects in graphite are expected to be smaller than in graphene, as the interaction between electrons and holes is more efficiently screened by the multiple layers¹⁶. Thus, a proper estimation of excitonic effects in graphene can be made only by directly measuring (or calculating) the response properties of the 2D layer surrounded by vacuum.

From a theoretical perspective, the dielectric response of freestanding graphene has been extensively studied with a variety of first-principles approaches based on density functional theory (DFT), and including many-body effects at different levels of theory. Starting from a DFT band structure, the energy-loss function at finite momentum transfer has been calculated mostly within the random-phase approximation (RPA)^{10-12,17-23}²⁴. DFT+RPA calculations accurately reproduce the experimental linear dispersion of the π plasmon only for momentum transfers along the graphene plane $\mathbf{q} > \mathbf{q}_c \simeq 0.1 \text{ \AA}^{-1}$, both in the ΓK and the ΓM directions^{10,11}.

Many-body effects stemming from electron-electron (e-e) and electron-hole (e-h) interactions have been analyzed, only for optical spectra, namely for vanishing transferred momentum²⁵⁻²⁷, within the GW approximation²⁸⁻³¹, accounting for repulsive e-e coupling in the band structure, and solving the Bethe-Salpeter equation (BSE)^{28,32,33} to include attractive e-h interactions. The inclusion of e-e effects strongly modifies the quasi-particle (QP) band structure, affecting not only the Dirac Fermi-velocity but also the energy gaps at the M and Γ points, and consequently the spectral position of the onset as well as of the π and $\pi + \sigma$ plasmons. Indeed, inclusion of QP corrections within the GW approach has proven crucial to predict Fermi velocities in better agreement with ARPES^{25,26,34}. On the other hand, the

larger QP gap at the M point due to e-e effects alone is responsible for a substantial blueshift of the π -plasmon peak in the calculated optical spectrum of graphene, with the predicted spectral position exceeding the experimental one by roughly 600 meV²⁵⁻²⁷. As shown by Yang et al.^{26,27}, for zero-momentum transfer the explicit inclusion of e-h coupling via BSE is then essential for reproducing the experimental peak position as well as the asymmetric profile of the excitations that gives rise to the π plasmon in EELS.

The importance of many-body and excitonic effects in the dielectric response of free-standing graphene can be anticipated by considering the reduced screening due to both its vanishing density of states at the Fermi level and its two-dimensional character³⁵. While the good agreement of DFT+RPA calculations of the π plasmon dispersion with experiments for $\mathbf{q} > \mathbf{q}_c$ has been tentatively ascribed to a cancellation of e-e and e-h effects¹⁰, it is still unknown how the sizeable excitonic and many-body effects that have been unveiled in the optical spectrum evolve in the finite-momentum regime.

In this work, we precisely address the regime of small, but finite, momentum transfers. EELS measurements of freestanding graphene have been performed in a transmission electron microscope (TEM) with unprecedented resolution both in energy and momentum to clearly separate the zero loss peak (ZLP) from the excitation gap of Dirac electrons. We focused on the low-energy (0-10 eV) EEL spectra in the $\mathbf{q} \leq 0.3 \text{ \AA}^{-1}$ range of momentum transfers. With the adopted setup, we were able to access not only the collective π -plasmon excitation, but also the onset of the particle-hole continuum, thus providing complementary information about excitonic effects on the two main spectral features in the considered momentum-energy range. Momentum-resolved EEL spectra have been simulated with first principles methods at increasing levels of theory, from the single-particle picture of the DFT+RPA calculations to GW computations accounting for many-body QP corrections, finally addressing excitonic effects and e-h interactions within BSE. This allowed us to assess the effects of e-e and e-h interactions separately by comparing spectra simulated at different approximation levels. Our comparative analysis unveils non-trivial momentum-dependent excitonic effects in the

dielectric response of graphene, whose signatures shape differently the EEL spectral features of both electron-hole pair and collective excitations.

Methods

Single layer graphene was synthesized by plasma-assisted chemical vapour deposition³⁷. The graphene layers were mechanically transferred to TEM grids. The samples were annealed *in situ* at 500°C overnight and kept at the same temperature during all measurements to maintain crystallinity and avoid surface contamination. The low magnification TEM image of the graphene on the TEM grid exhibits a free-standing area with a hole diameter of approximately 1 μm [Fig. 1(a)]. The typical crystal structure of the sample and its Fast Fourier Transform (FFT) image are presented in Fig. 1 (b) and (c), respectively. Both images show a defect free single crystal in a $10 \times 10 \text{ nm}^2$ wide region. Fig. 1 (d) is the lower magnified overview diffraction image that was used to position the aperture in the diffraction plane. The positioning and beam drift control before and after each acquisition are checked in the low magnification diffraction pattern. They are intrinsically limited to the pixel size of 0.004 \AA^{-1} . The spectral resolution of $\pm 0.02 \text{ \AA}^{-1}$ is achieved with a longer camera length (215 cm). EEL spectra were measured at 30 kV in a JEOL TEM (3C2) equipped with a Schottky field emission gun, a double Wien filter monochromator and delta correctors. The energy resolution was set to 45 meV in full width half maximum (FWHM). A collimated 500 nm wide beam ($\mathbf{q} \leq 0.006 \text{ \AA}^{-1}$) was formed in imaging mode. The incident beam was perpendicular to the graphene layer, and the diffraction plane was formed with a camera length of 215 cm. A pin-hole type aperture ($\pm 0.015 \text{ \AA}^{-1}$) was inserted in the diffraction plane. The beam current was approximately 10 pA. The EEL spectra were collected from multiple \mathbf{q} along ΓK and ΓM with a low-voltage optimized GATAN GIF quantum spectrometer. The spectra are sums of 300 individual acquisitions. The dwell time ranges between 0.01 s (for $\mathbf{q}=0.015 \text{ \AA}^{-1}$) to 2 sec (for $\mathbf{q}=0.3 \text{ \AA}^{-1}$). The zero-loss peak (ZLP) is clearly separated from

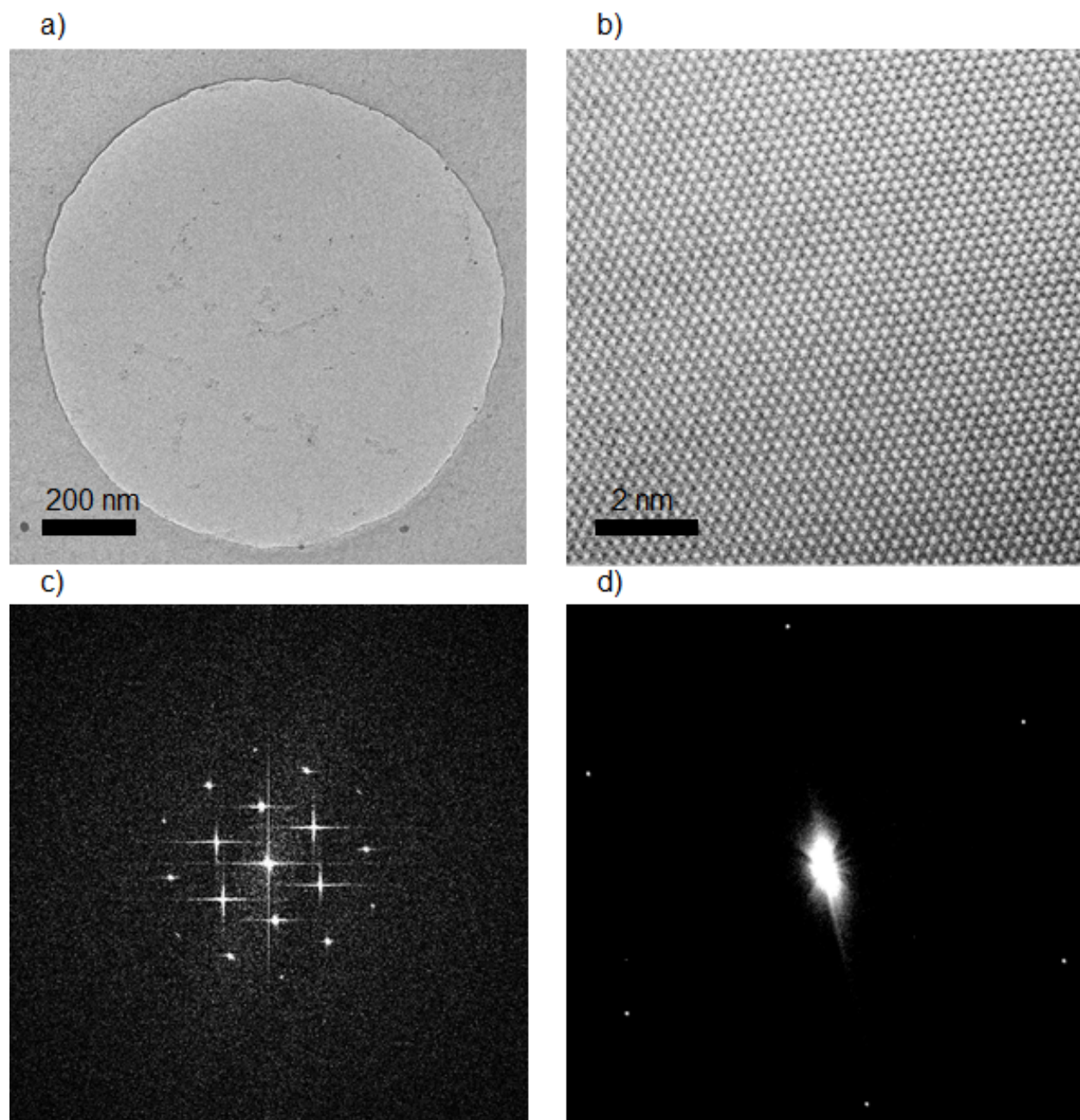


Figure 1: TEM images and diffraction pattern of freestanding graphene at 30 keV. (a): low-magnification TEM image. (b): high resolution TEM image. (c): FFT of the high resolution image in (b). (d): diffraction pattern of a 500 nm wide beam acquired at a camera length of 40 cm.

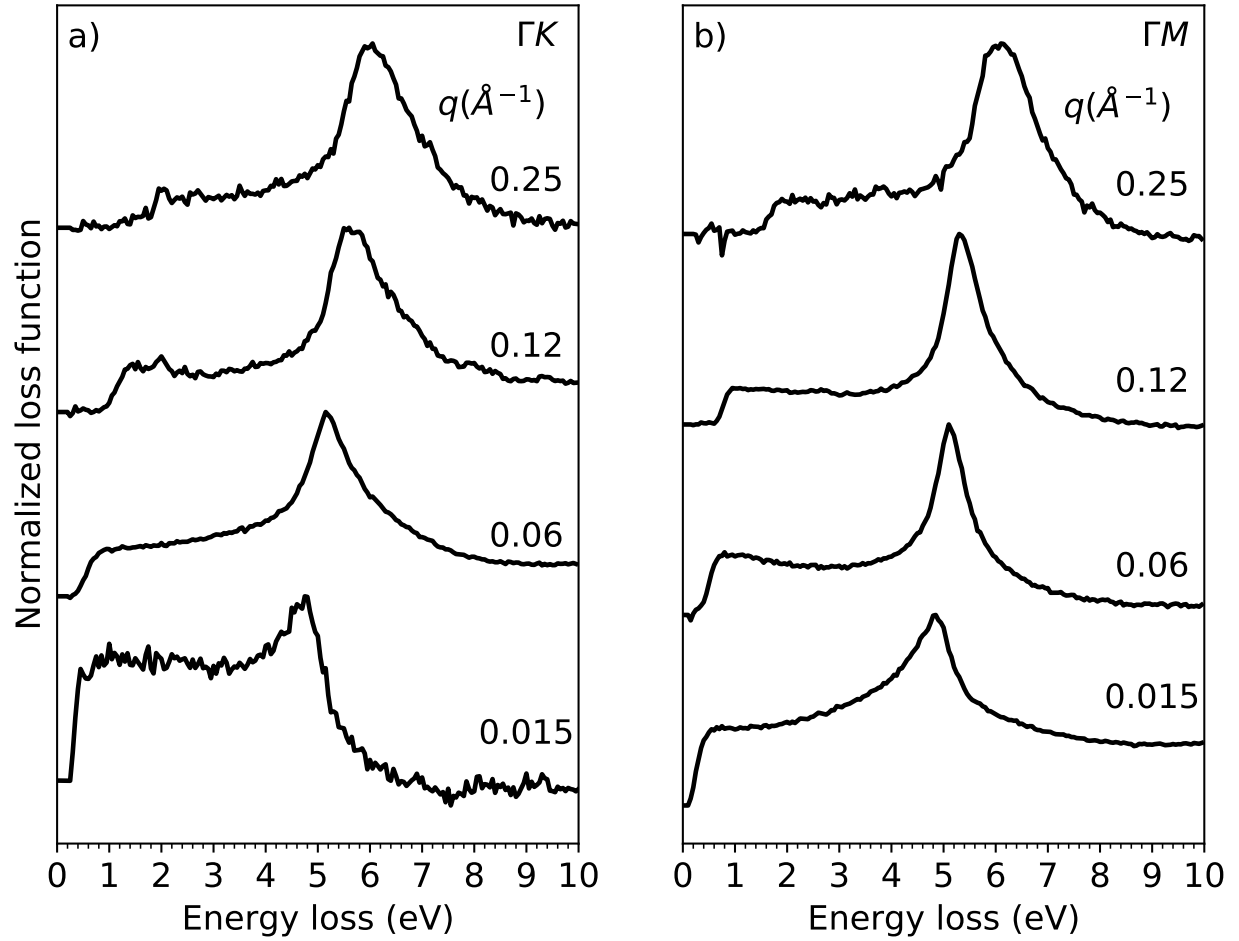


Figure 2: Measured low energy loss spectra of freestanding graphene for different momentum transfers \mathbf{q} oriented along the ΓK (a) and ΓM (b) directions. The zero loss peak has been removed (see text). The complete set of measured spectra is included in the SM³⁶.

the onset (i.e. the excitation gap) for $\mathbf{q} > 0.05 \text{ \AA}^{-1}$. At smaller \mathbf{q} , the onset overlap with the tails of the ZLP. At all momentum transfers, we modelled the ZLP with an inverse power law^{38,39}, and removed as described in the supplementary material (SM)³⁶. In Fig. 5, black stars correspond to data where the ZLP is clearly separated from the onset, while grey stars ($\mathbf{q} < 0.05 \text{ \AA}^{-1}$) correspond to onsets that have only become visible after the ZLP subtraction, and their uncertainties are on the order of the onset itself.

DFT calculations were performed using a plane wave basis set as implemented in the QUANTUM ESPRESSO package⁴⁰, with the local density approximation⁴¹. The YAMBO code^{42,43} has been adopted to compute the quasi-particle band structure, within the G_0W_0 approximation, and the EEL spectra, calculated at different levels of theory, considering DFT and GW QP energy levels within the RPA and the BSE response functions. In all cases, finite- \mathbf{q} simulations have been performed. The adopted supercell includes a vacuum region along the perpendicular direction of 10 \AA , and a 2D slab Coulomb cutoff^{44,45} has been used to avoid spurious interactions. For GW calculations, we adopted the plasmon-pole approximation in the Godby-Needs scheme⁴⁶. The long-wavelength limit of the semimetallic screening contribution have been included analytically within the Dirac cone model (see SM³⁶). Excitation broadening, mainly originating from electron-phonon coupling, has been included through the model described in Ref.⁴⁷. Further details can be found in the SM³⁶.

Results

The measured low-energy (0-10 eV) loss spectra are shown in Fig. 2 for selected momentum transfers \mathbf{q} along the ΓK and ΓM directions. As expected, a peak due to the π plasmon is present at about 5-6 eV. Notably, a clear finite momentum-dependent onset is present in all the measured spectra. To our knowledge, this is the first direct experimental evidence of such onset dispersion for freestanding graphene at such low momentum transfers (see below for a detailed discussion). Interestingly, the line shape of the π plasmon shows a transition from an

asymmetric profile with a tail towards lower energies in the low momentum-transfer regime, to a symmetric shape around $\mathbf{q} = 0.06 \text{ \AA}^{-1}$, and finally a reversed asymmetric profile leaning towards higher energies for $\mathbf{q} > \mathbf{q}_c$. Spectral features are found to be essentially independent of the crystallographic direction in the measured momentum range, consistent with previous reports^{9,11}.

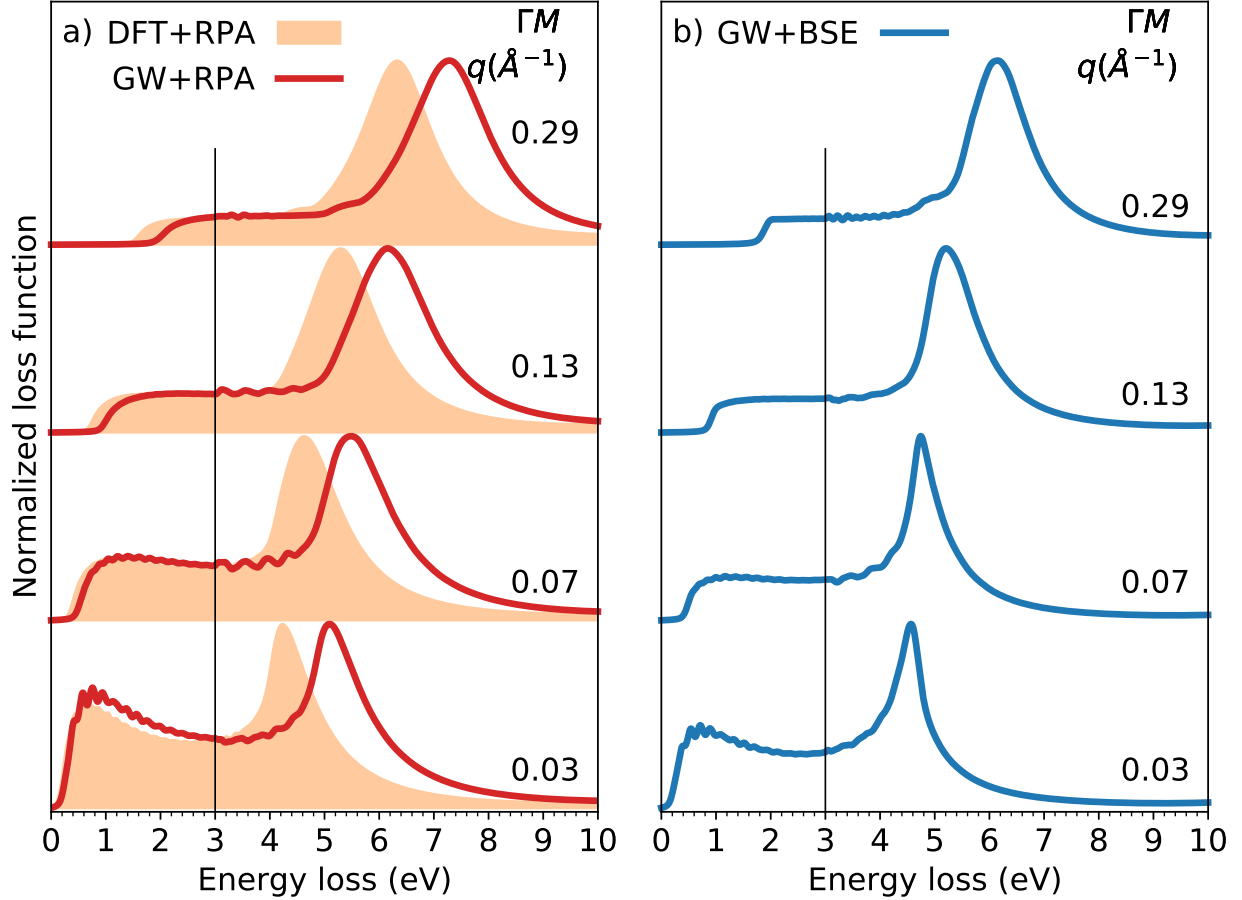


Figure 3: Energy loss spectra of freestanding graphene at increasing momentum transfers along ΓM calculated at different theory levels: DFT+RPA and GW+RPA (a), GW+BSE (b). For all the spectra, an energy dependent broadening has been considered to describe relaxation processes due to electron-phonon coupling, according to Eqn. (14) of Ref.⁴⁷. The vertical black lines in the panels (b,c) separate the regions for different convergence parameters (see text).

In order to investigate the origin of the observed experimental features, we compare the measured data with first principle calculations of the loss function. In Fig. 3, we show EEL spectra calculated at different levels of theory along the ΓM direction (calculations for

more \mathbf{q} are included in the SM³⁶). The first+second acronym in the labels refers to the level of theory used for the band structure+response function. In panel (a) we report the loss function computed at the DFT+RPA level (orange shaded area), which, as an effective single particle picture, we then use as a starting point to understand many-body effects. The inclusion of GW corrections in the band structure (GW+RPA), red line in panel (a), result in an almost rigid blue-shift of the π -plasmon peak. Instead, when including e-h coupling effects using GW+BSE, the peaks are shifted and the shape is modified in a non uniform way, as clearly seen in Fig. 3(b). In particular, one can recognize that the experimentally observed changes in the asymmetry of the plasmon peak can only be reproduced by including electron-hole interaction effects (GW+BSE).

This scenario is even more evident by looking at Fig. 4, where we compare the features of the π plasmon obtained experimentally and from *ab initio* calculations. The independent particle picture (DFT+RPA) is not able to reproduce the experimental dispersion below $\mathbf{q}_c \simeq 0.1 \text{ \AA}^{-1}$, as already pointed out in Refs.^{10,11}. The DFT+RPA dispersion is in fact quadratic in the low-momentum regime, transitioning to a linear behaviour closely matching to experiments for $\mathbf{q} > \mathbf{q}_c$. The GW corrections to the band structure near M (i.e. the relevant BZ region for what concerns the π plasmon) enlarge the gap by about 0.88 eV. Thus, the inclusion of e-e interaction within GW+RPA determines a rigid blue shift that reproduces well the experimental optical limit, but fails for finite \mathbf{q} and in keeping a parabolic dispersion for small momenta.

Excitonic effects (included via BSE) produce instead a momentum-dependent red shift, that increases with \mathbf{q} before it saturates around \mathbf{q}_c . Such a momentum-dependent effect due to e-h interaction is responsible for the linear dispersion of the π plasmon in the GW+BSE results (blue symbols and line in Fig. 4a), which reproduces the experimental trend well. In Fig. 4(b,c) we compare the measured and calculated shapes of the π -plasmon peak at $\mathbf{q} = 0.06 \text{ \AA}^{-1}$ and $\mathbf{q} = 0.13 \text{ \AA}^{-1}$, respectively, by shifting the plasmon peak so that its center is located at $\omega = 0$. DFT-RPA data show in both cases a peak that is too broad, with less

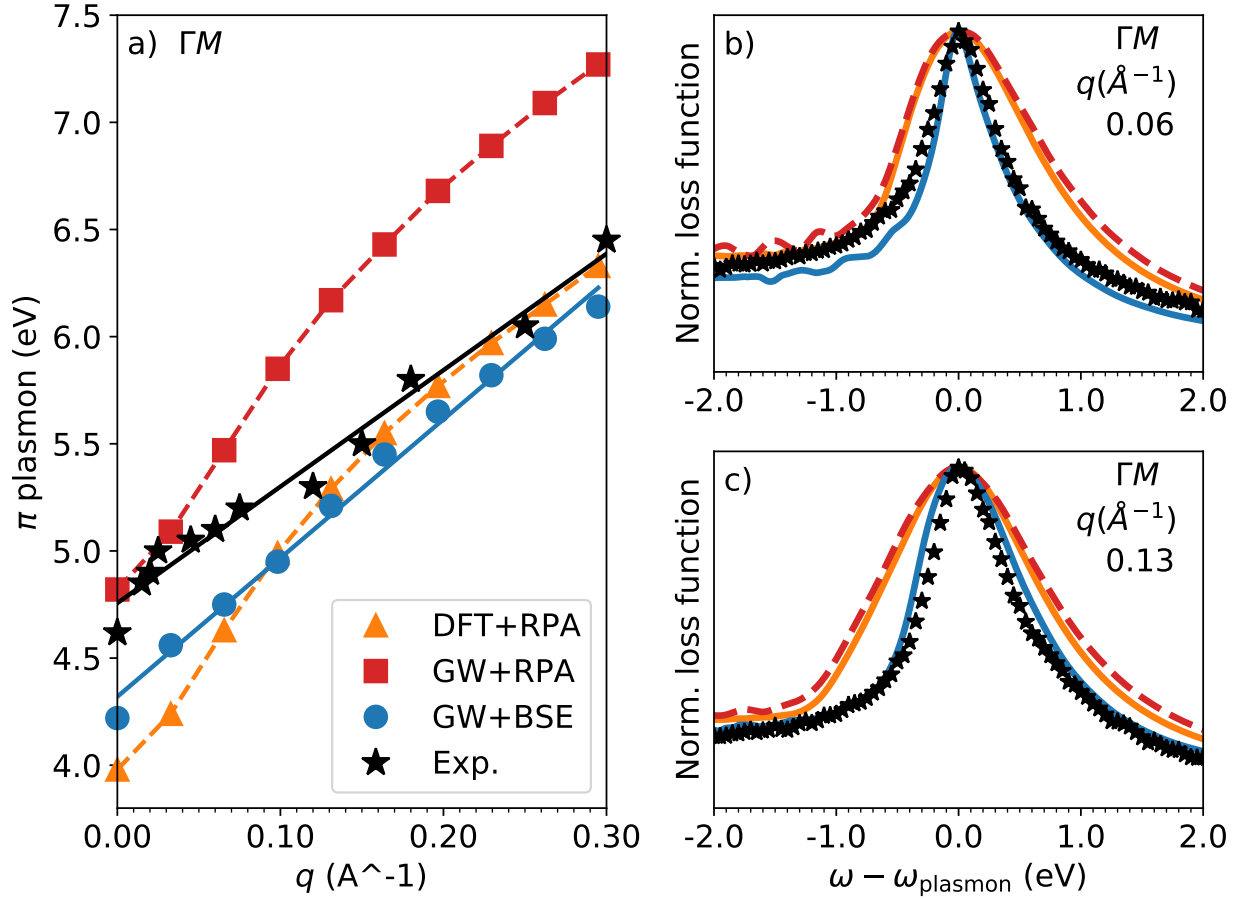


Figure 4: (a): π -plasmon dispersion obtained with the procedure described in the SM³⁶. The straight line in black (blue) is a linear regression of the measured (calculated) plasmon dispersion. Dashed lines are a guide to the eye. (b, c): measured and calculated π -plasmon peaks of freestanding graphene at different momentum transfers along the ΓM direction. (b): $\mathbf{q} = 0.06 \text{\AA}^{-1}$; (c): $\mathbf{q} = 0.13 \text{\AA}^{-1}$. Different colours refer to different theory levels in the calculation: DFT+RPA (orange lines), GW+RPA (red lines) and GW+BSE (blue lines). Experimental data are shown as black stars.

asymmetric features. The inclusion of the e-e interaction (GW+RPA) does not influence the peak shape. Instead, the peak reshaping is a feature provided by the e-h interaction, as it can be seen from the nearly perfect match between experimental and GW+BSE results.

We are now in the position to discuss the low energy features of the EELS data, notably including the onset dispersion observed experimentally (see Fig. 2). In particular, in Fig. 5 we analyse the position and shape of the onset spectral structures, related to the e-h pair excitation gap obtained at finite momentum transfer \mathbf{q} , as expected from the semimetallic nature of freestanding graphene. The position of the onset is extracted from experimental data by considering the tangent at half-height of the onset structure, and then taking the intercept with the horizontal axis (see Fig. 5b). The same procedure is applied also to the theoretical data. With these definitions, it is evident (Fig. 5a,b) that the onset position is sensibly dependent on the choice of the theory level used to describe the band structure. Indeed, the inclusion of e-e interactions (GW corrections) significantly enlarge the gap opening with a higher Fermi velocity.

In Fig. 5(b) we show the onset shape at $\mathbf{q} = 0.20 \text{ \AA}^{-1}$. While the onset position is similar in the GW+RPA and GW+BSE cases, it is evident that e-h interaction modifies the onset shape, providing a better agreement with experiments. We have explicitly verified that this feature mainly originates from matrix element effects, i.e. the excitonic eigenvalues (DOS) are mostly unchanged while the red shift comes from a redistribution of their spectral weights. Also in this case, the GW+BSE calculations consistently produce dispersions in excellent agreement with experiments, as shown in Fig. 5(d). In Fig. 5(c) we compare our current onset positions with those extracted from Ref. ¹⁰. The red disk in the sketched Brillouin zone (BZ) marks the range $\mathbf{q} < 0.4 \text{ \AA}^{-1}$, where the spectral onset could not be accessed in Ref. ¹⁰. Here we pushed this accessibility limit down to $\mathbf{q} \leq 0.05 \text{ \AA}^{-1}$ (grey disk and range) in Fig. 5(d). The measured onsets with $\mathbf{q} \leq 0.05 \text{ \AA}^{-1}$ are dependent on the details of the ZLP subtraction and marked grey. Their errors are comparable to the gap opening. The anisotropy in the onset dispersion along the ΓM and ΓK directions in panels (c) and (d)

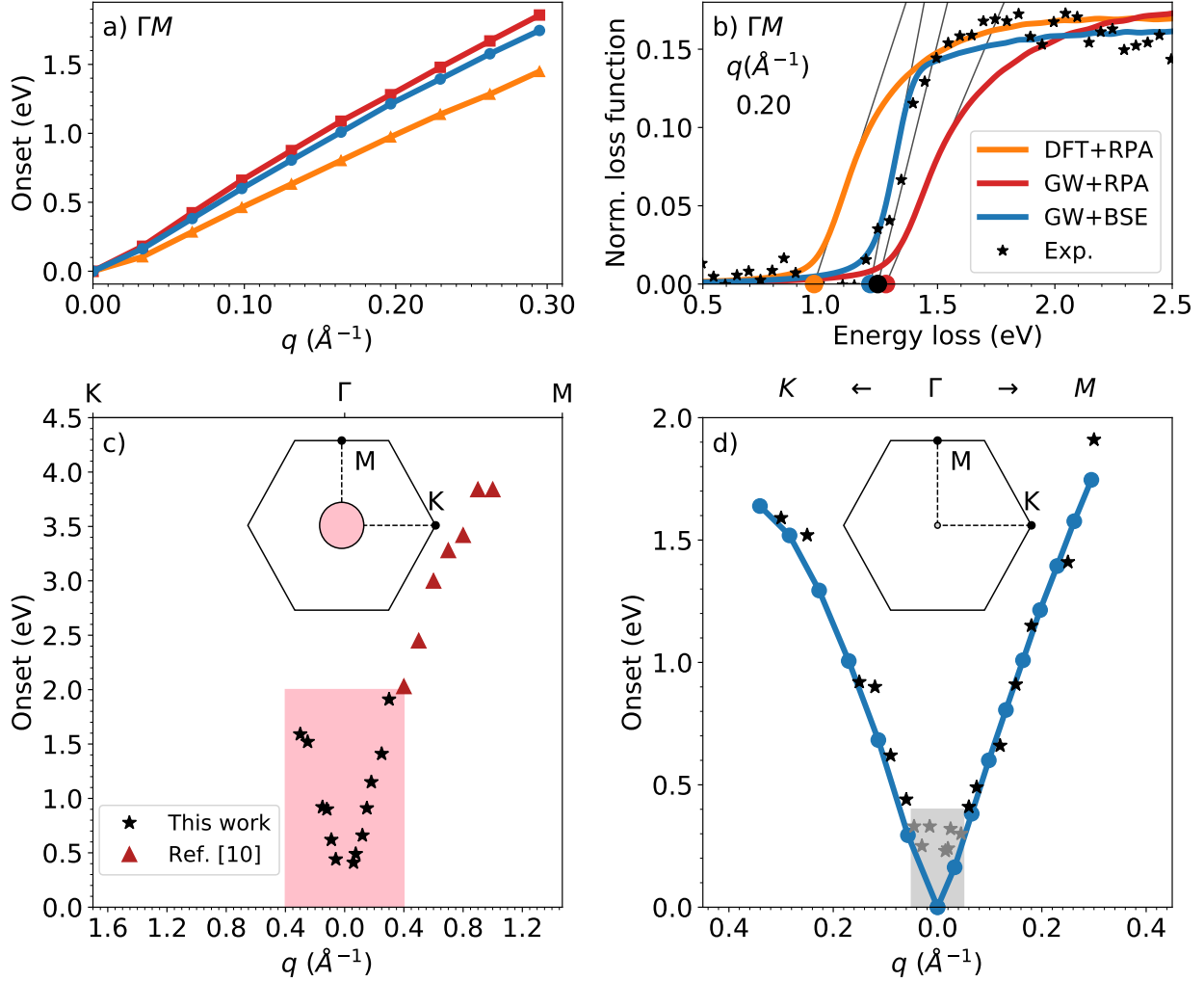


Figure 5: (a): onset dispersion of freestanding graphene along the ΓM direction calculated at different theory levels. (b): experimental and calculated onset shape at $\mathbf{q} \approx 0.2 \text{ \AA}^{-1}$. Grey lines indicate the half-height tangent used in the determination of the onset. Filled circles indicate the onset positions. (c): measured onsets for \mathbf{q} in ΓK and ΓM directions. We extracted from Ref. ¹⁰ onset positions at high momentum transfer along the ΓM direction. The extraction has not been done in the ΓK direction due to experiential uncertainties. The onset inaccessible region of Ref. ¹⁰ ($\mathbf{q} \leq 0.4 \text{ \AA}^{-1}$) has been tinted in red. It is also shown inside the first BZ of graphene. (d): zoom of the measured onset dispersion (black) and comparison with the calculated onset (blue). Our range of inaccessible $\mathbf{q} \leq 0.05 \text{ \AA}^{-1}$ is tinted in grey and is also shown within the first BZ. The grey data points within $\mathbf{q} \leq 0.05 \text{ \AA}^{-1}$ have large errors as they depend on the removal of the ZLP.

arises from the trigonal warping of the Dirac cones.

Conclusions

We performed momentum-resolved EELS measurements of freestanding graphene in a TEM with a high energy and momentum resolution, that is the key to disentangle the near optical excitations of Dirac electrons from the quasielastic scattering in the low momentum-transfer regime, allowing us to resolve a number of spectral features as well as the dispersive nature of excitonic effects in graphene. Jointly, we perform *ab initio* calculations of the loss function at different levels of theory, ranging from DFT+RPA to GW+BSE. The comparison between measurements and *ab initio* calculations allows us to unravel the physical origins behind the observed spectral features, namely position and shape of the π -plasmon peak and the spectral onset.

For what concerns the π plasmon dispersion, we found that the inclusion of electron-electron interactions at the GW level provides an almost rigid blue-shift of the peaks that is independent of the momentum transfer, such that this correction alone does not help in reproducing the experimentally observed features. Instead, the further inclusion of electron hole-attraction provides an unexpected momentum-dependent red-shift, that is responsible for the linear plasmon peak dispersion clearly observed in experiments. The asymmetric shapes of the π -plasmon peak can also only be ascribed to excitonic effects, as already shown in optics. The dispersion of the onset as a function of the transferred momentum is already in quantitative agreement with experiments once the electron-electron interaction is included. However, excitonic effects still play a fundamental role in describing the onset shape.

Acknowledgement

RS, YCL and KS acknowledge the support from JST-CREST (JPMJCR20B1, JPMJCR20B5, JPMJCR1993), JST-PRESTO (JPMJPR2009), and JSPS-KAKENHI (JP21H05235, JP22H05478, JP23H00277). This project has received funding from the European Research Council (ERC) under the European Union’s Horizon 2020 research and innovation program (MORE-TEM ERC-SYN project, grant agreement No 951215). DV, AF and AG acknowledge the support from MaX – MAterials design at the eXascale – a European Centre of Excellence funded by the European Union’s program HORIZON-EUROHPC-JU-2021-COE-01 (Grant No. 101093374), ICSC – Centro Nazionale di Ricerca in High Performance Computing, Big Data and Quantum Computing, funded by European Union –NextGenerationEU - PNRR, Missione 4 Componente 2 Investimento 1.4 and the Italian national program PRIN2017 2017BZPKSZ “Excitonic insulator in two-dimensional long-range interacting systems”. We acknowledge CINECA for computational resources, awarded via the ISCRA Grants No. HP10BKBJMI and HP10BV0TBS

References

- (1) Novoselov, K. S.; Geim, A. K.; Morozov, S. V.; Jiang, D.; Zhang, Y.; Dubonos, S. V.; Grigorieva, I. V.; Firsov, A. A. Electric Field Effect in Atomically Thin Carbon Films. Science **2004**, 306, 666–669.
- (2) Novoselov, K. S.; Geim, A. K.; Morozov, S. V.; Jiang, D.; Katsnelson, M. I.; Grigorieva, I. V.; Dubonos, S. V.; Firsov, A. A. Two-dimensional gas of massless Dirac fermions in graphene. Nature **2005**, 438, 197–200.
- (3) Castro Neto, A. H.; Guinea, F.; Peres, N. M. R.; Novoselov, K. S.; Geim, A. K. The electronic properties of graphene. Rev. Mod. Phys. **2009**, 81, 109–162.

- (4) Bonaccorso, F.; Sun, Z.; Hasan, T.; Ferrari, A. C. Graphene photonics and optoelectronics. Nature Photonics **2010**, 4, 611.
- (5) Grigorenko, A.; Polini, M.; Novoselov, K. Graphene plasmonics. Nature Photon. **2012**, 6, 749–758.
- (6) García de Abajo, F. J. Graphene Plasmonics: Challenges and Opportunities. ACS Photonics **2014**, 1, 135–152.
- (7) Taft, E. A.; Philipp, H. R. Optical Properties of Graphite. Phys. Rev. **1965**, 138, A197–&.
- (8) Zeppenfeld, K. Anisotropic Plasmon Behaviour in Graphite. Phys. Lett. A **1967**, 25, 335–+.
- (9) Kinyanjui, M. K.; Kramberger, C.; Pichler, T.; Meyer, J. C.; Wachsmuth, P.; Benner, G.; Kaiser, U. Direct probe of linearly dispersing 2D interband plasmons in a free-standing graphene monolayer. Europhys. Lett. **2012**, 97, 57005.
- (10) Wachsmuth, P.; Hambach, R.; Kinyanjui, M. K.; Guzzo, M.; Benner, G.; Kaiser, U. High-energy collective electronic excitations in free-standing single-layer graphene. Phys. Rev. B **2013**, 88, 075433.
- (11) Wachsmuth, P.; Hambach, R.; Benner, G.; Kaiser, U. Plasmon bands in multilayer graphene. Phys. Rev. B **2014**, 90, 235434.
- (12) Kramberger, C.; Hambach, R.; Giorgetti, C.; Rummeli, M. H.; Knupfer, M.; Fink, J.; Buchner, B.; Reining, L.; Einarsson, E.; Maruyama, S.; Sottile, F.; Hannewald, K.; Olevano, V.; Marinopoulos, A. G.; Pichler, T. Linear plasmon dispersion in single-wall carbon nanotubes and the collective excitation spectrum of graphene. Phys. Rev. Lett. **2008**, 100, 196803.

- (13) Laitenberger, P.; Palmer, R. E. Plasmon Dispersion and Damping at the Surface of a Semimetal. Phys. Rev. Lett. **1996**, 76, 1952–1955.
- (14) Reed, J. P.; Uchoa, B.; Joe, Y. I.; Gan, Y.; Casa, D.; Fradkin, E.; Abbamonte, P. The Effective Fine-Structure Constant of Freestanding Graphene Measured in Graphite. Science **2010**, 330, 805–808.
- (15) Gan, Y.; de la Peña, G. A.; Kogar, A.; Uchoa, B.; Casa, D.; Gog, T.; Fradkin, E.; Abbamonte, P. Reexamination of the effective fine structure constant of graphene as measured in graphite. Phys. Rev. B **2016**, 93, 195150.
- (16) Trevisanutto, P. E.; Holzmann, M.; Côté, M.; Olevano, V. Ab initio high-energy excitonic effects in graphite and graphene. Phys. Rev. B **2010**, 81, 121405.
- (17) Yan, J.; Thygesen, K. S.; Jacobsen, K. W. Nonlocal Screening of Plasmons in Graphene by Semiconducting and Metallic Substrates: First-Principles Calculations. Phys. Rev. Lett. **2011**, 106, 146803.
- (18) Despoja, V.; Dekanić, K.; Šunjić, M.; Marušić, L. Ab initio study of energy loss and wake potential in the vicinity of a graphene monolayer. Phys. Rev. B **2012**, 86, 165419.
- (19) Despoja, V.; Novko, D.; Dekanić, K.; Šunjić, M.; Marušić, L. Two-dimensional and π plasmon spectra in pristine and doped graphene. Phys. Rev. B **2013**, 87, 075447.
- (20) Mowbray, D. J. Theoretical electron energy loss spectroscopy of isolated graphene. Physica Status Solidi (b) **2014**, 251, 2509–2514.
- (21) Novko, D.; Despoja, V.; Šunjić, M. Changing character of electronic transitions in graphene: From single-particle excitations to plasmons. Phys. Rev. B **2015**, 91, 195407.
- (22) Nazarov, V. U. Electronic excitations in quasi-2D crystals: what theoretical quantities are relevant to experiment? New J. Phys. **2015**, 17, 073018.

- (23) Li, P.; Ren, X.; He, L. First-principles calculations and model analysis of plasmon excitations in graphene and graphene/hBN heterostructure. Phys. Rev. B **2017**, 96, 165417.
- (24) Zheng, H.; Gan, Y.; Abbamonte, P.; Wagner, L. K. Importance of σ Bonding Electrons for the Accurate Description of Electron Correlation in Graphene. Phys. Rev. Lett. **2017**, 119, 166402.
- (25) Trevisanutto, P. E.; Giorgetti, C.; Reining, L.; Ladisa, M.; Olevano, V. Ab Initio *GW* Many-Body Effects in Graphene. Phys. Rev. Lett. **2008**, 101, 226405.
- (26) Yang, L.; Deslippe, J.; Park, C.-H.; Cohen, M. L.; Louie, S. G. Excitonic Effects on the Optical Response of Graphene and Bilayer Graphene. Phys. Rev. Lett. **2009**, 103, 186802.
- (27) Yang, L. Excitons in intrinsic and bilayer graphene. Phys. Rev. B **2011**, 83, 085405.
- (28) Hedin, L. New Method for Calculating the One-Particle Green's Function with Application to the Electron-Gas Problem. Phys. Rev. **1965**, 139, A796–A823.
- (29) Strinati, G.; Mattausch, H. J.; Hanke, W. Dynamical aspects of correlation corrections in a covalent crystal. Phys. Rev. B **1982**, 25, 2867–2888.
- (30) Hybertsen, M. S.; Louie, S. G. Electron correlation in semiconductors and insulators: Band gaps and quasiparticle energies. Phys. Rev. B **1986**, 34, 5390–5413.
- (31) Godby, R. W.; Schlüter, M.; Sham, L. J. Self-energy operators and exchange-correlation potentials in semiconductors. Phys. Rev. B **1988**, 37, 10159–10175.
- (32) Strinati, G. Application of the Green's functions method to the study of the optical properties of semiconductors. La Rivista del Nuovo Cimento (1978-1999) **1988**, 11, 1–86.

- (33) Onida, G.; Reining, L.; Rubio, A. Electronic excitations: density-functional versus many-body Green's-function approaches. Rev. Mod. Phys. **2002**, 74, 601–659.
- (34) Attaccalite, C.; Rubio, A. Fermi velocity renormalization in doped graphene. Physica Status Solidi (b) **2009**, 246, 2523–2526.
- (35) Thygesen, K. S. Calculating excitons, plasmons, and quasiparticles in 2D materials and van der Waals heterostructures. 2D Materials **2017**, 4, 022004.
- (36) See Supplemental Material for detailed information about the experimental and theoretical methods and data analysis.
- (37) Kato, R.; Minami, S.; Koga, Y.; Hasegawa, M. High growth rate chemical vapor deposition of graphene under low pressure by RF plasma assistance. Carbon **2016**, 96, 1008 – 1013.
- (38) Krivanek, O. L.; Lovejoy, T. C.; Dellby, N.; Aoki, T.; Carpenter, R. W.; Rez, P.; Soignard, E.; Zhu, J.; Batson, P. E.; Lagos, M. J.; Egerton, R. F.; Crozier, P. A. Vibrational spectroscopy in the electron microscope. Nature **2014**, 514, 209–212.
- (39) Hachtel, J. A.; Lupini, A. R.; Idrobo, J. C. Exploring the capabilities of monochromated electron energy loss spectroscopy in the infrared regime. Scientific reports **2018**, 8, 5637.
- (40) Giannozzi, P.; Baseggio, O.; Bonfà, P.; Brunato, D.; Car, R.; Carnimeo, I.; Cavazzoni, C.; de Gironcoli, S.; Delugas, P.; Ferrari Ruffino, F.; Ferretti, A.; Marzari, N.; Timrov, I.; Urru, A.; Baroni, S. Quantum ESPRESSO toward the exascale. J. Chem. Phys. **2020**, 152, 154105.
- (41) Perdew, J. P.; Zunger, A. Self-interaction correction to density-functional approximations for many-electron systems. Phys. Rev. B **1981**, 23, 5048–5079.
- (42) Marini, A.; Hogan, C.; Grüning, M.; Varsano, D. yambo: An ab initio tool for excited state calculations. Comput. Phys. Commun. **2009**, 180, 1392 – 1403.

- (43) Sangalli, D. et al. Many-body perturbation theory calculations using the yambo code. J. Phys.: Condens. Matter **2019**, 31, 325902.
- (44) Ismail-Beigi, S. Truncation of periodic image interactions for confined systems. Phys. Rev. B **2006**, 73, 233103.
- (45) Rozzi, C. A.; Varsano, D.; Marini, A.; Gross, E. K. U.; Rubio, A. Exact Coulomb cutoff technique for supercell calculations. Phys. Rev. B **2006**, 73, 205119.
- (46) Godby, R. W.; Needs, R. J. Metal-insulator transition in Kohn-Sham theory and quasi-particle theory. Phys. Rev. Lett. **1989**, 62, 1169–1172.
- (47) Venezuela, P.; Lazzeri, M.; Mauri, F. Theory of double-resonant Raman spectra in graphene: Intensity and line shape of defect-induced and two-phonon bands. Phys. Rev. B **2011**, 84, 035433.